Human *GNPTAB* stuttering mutations engineered into mice cause vocalization deficits and astrocyte pathology in the corpus callosum

Tae-Un Han[a], Jessica Root[a], Laura D. Reyes[b], Elizabeth B. Huchinson[b], Johann du Hoffmann[c], Wang-Sik Lee[d], Terra D. Barnes[e], and Dennis Drayna[a,1]

[a]Section on Genetics of Communication Disorders, National Institute on Deafness and Other Communication Disorders, National Institutes of Health, Bethesda, MD 20892; [b]Section on Quantitative Medical Imaging, National Institute of Biomedical Imaging and Bioengineering, National Institutes of Health, Bethesda, MD 20892; [c]Section on Behavioral Neuroscience, Rodent Behavioral Core, National Institute of Mental Health, National Institutes of Health, Bethesda, MD 20892; [d]Department of Internal Medicine, Washington University School of Medicine in St. Louis, St. Louis, MO 63110; and [e]Department of Neuroscience, Washington University School of Medicine in St. Louis, St. Louis, MO 63110

Edited by Stephen T. Warren, Emory University School of Medicine, Atlanta, GA, and approved July 18, 2019 (received for review January 28, 2019)

Stuttering is a common neurodevelopmental disorder that has been associated with mutations in genes involved in intracellular trafficking. However, the cellular mechanisms leading to stuttering remain unknown. Engineering a mutation in *N*-acetylglucosamine-1-phosphate transferase subunits α and β (GNPTAB) found in humans who stutter into the mouse *Gnptab* gene resulted in deficits in the flow of ultrasonic vocalizations similar to speech deficits of humans who stutter. Here we show that other human stuttering mutations introduced into this mouse gene, *Gnptab* Ser321Gly and Ala455Ser, produce the same vocalization deficit in 8-day-old pup isolation calls and do not affect other nonvocal behaviors. Immunohistochemistry showed a marked decrease in staining of astrocytes, particularly in the corpus callosum of the *Gnptab* Ser321Gly homozygote mice compared to wild-type littermates, while the staining of cerebellar Purkinje cells, oligodendrocytes, microglial cells, and dopaminergic neurons was not significantly different. Diffusion tensor imaging also detected deficits in the corpus callosum of the *Gnptab* Ser321Gly mice. Using a range of cell type-specific Cre-drivers and a *Gnptab* conditional knockout line, we found that only astrocyte-specific *Gnptab*-deficient mice displayed a similar vocalization deficit. These data suggest that vocalization defects in mice carrying human stuttering mutations in *Gnptab* derive from abnormalities in astrocytes, particularly in the corpus callosum, and provide support for hypotheses that focus on deficits in interhemispheric communication in stuttering.

stuttering | astrocytes | white matter | mouse vocalization | Cre-drivers

Stuttering is a common neurodevelopmental disorder characterized by disruptions in the fluent flow of speech (1), typically in the absence of other neurological deficits. Stuttering displays high heritability (2), and recent studies have identified mutations in the *GNPTAB*, *GNPTG*, *NAGPA*, and *AP4E1* genes that are associated with this disorder (3–5). The products of these genes interact with each other in vivo and in vitro (3, 4), and participate in the control of intracellular trafficking, deficits in which are recognized in a wide range of neurological disorders (6).

A primary goal for stuttering research has been to understand the neuropathology underlying this disorder. Imaging studies have identified differences in the brains of individuals who stutter (7–10). However, such studies have been limited by the difficulty of determining whether these differences are the cause of stuttering or the result of stuttering, and by the fact that they do not provide resolution at the cellular and molecular level. The identification of mutations in specific genes associated with human stuttering has allowed the construction of mouse models of the disorder. Mice display rich, context-specific ultrasonic vocalizations (USVs) that have become increasingly well characterized (11–14) and have been found to be under substantial genetic control (15–17). In addition, the brain anatomy and circuitry for vocalization in the mouse has been shown to share similarities with those of humans (18). In addition, mice carrying mutations in *FoxP2*, a gene mutated in human developmental verbal dyspraxia, have been shown to have abnormalities in a range of vocalization phenotypes (19, 20), supporting the view that mice can serve as a valid model for investigating central nervous system functions associated with the control of vocalization. Aided by our increasing understanding of mouse vocalization, we have generated a mouse model of stuttering by engineering a common stuttering mutation in the *Gnptab* gene encoding *N*-acetylglucosamine-1-phosphate transferase subunits α and β (21) into the mouse germline. While the ultrasonic pup isolation calls of such mice display many normal features, they have abnormally long pauses in their stream of vocalization compared to their wild-type littermates, and these abnormal pauses are similar to those observed in the speech of the humans who carry such mutations (22).

In this study, we sought to confirm and expand our understanding of the effects of *GNPTAB* mutations found in human stuttering on mouse USV, and to use such mutant mice to investigate the neuropathology present in these animals. To do this, we introduced additional human stuttering mutations in *Gnptab*

Significance

Stuttering is a common neurodevelopmental disorder. However, the neurological causes of this disorder are poorly understood. The disorder is highly genetic, and recent discoveries have found several genes involved in this disorder, but how these lead to the unique clinical features of stuttering has been unknown. We have shown that mice carrying human stuttering mutations display vocalization deficits that recreate the salient features of human stuttering. In these mice, we have used several different complementary techniques to identify a specific deficit in astrocytes, a type of glial cell prominent in white matter tracts, particularly in the corpus callosum of these mice. These findings suggest astrocytes as a site of the neuropathology, leading to a deficit in interhemispheric connectivity in stuttering.

Author contributions: T.-U.H., J.d.H., and D.D. designed research; T.-U.H., J.R., L.D.R., E.B.H., and W.-S.L. performed research; T.-U.H. contributed new reagents/analytic tools; T.-U.H., J.R., E.B.H., J.d.H., W.-S.L., T.D.B., and D.D. analyzed data; and T.-U.H., J.d.H., and D.D. wrote the paper.

The authors declare no conflict of interest.

This article is a PNAS Direct Submission.

[1]To whom correspondence may be addressed. Email: drayna@nidcd.nih.gov.

This article contains supporting information online at www.pnas.org/lookup/suppl/doi:10.1073/pnas.1901480116/-/DCSupplemental.

Published online August 12, 2019.

into mice and tested the USVs in these mice. We performed immunohistochemistry studies of the brains of these animals, focusing on cell types and brain regions previously suggested to be involved in human stuttering. To obtain orthogonal evidence regarding the role of brain regions and cell types in the disordered vocalizations of mice carrying human stuttering mutations, we selectively knocked out the *Gnptab* gene in specific brain cell types or lineages using a range of neuronal Cre-driver mouse strains (23, 24), and tested the USVs in these animals.

Results

Abnormal USVs in Knockin Mice Carrying Mutations Found in Human Stuttering. A previous study of mice carrying the human stuttering mutation *GNPTAB* Glu1200Lys in the orthologous mouse *Gnptab* gene showed that vocalization anomalies of mutant mice were most pronounced at postnatal days 3 to 8 (P3 to P8) (22). We recorded these pup isolation calls at P8 and analyzed their rates, spectral characteristics, and timing. Barnes et al. (22) found differences in the timing of vocalizations between homozygote mutant (mut/mut) and their wild-type littermates, with increased pauses between bouts of syllables in mutant mice and abnormally long pauses in the stream of their vocalization that are similar to those detected using a quantitative analysis of the vocalizations of humans who stutter carrying such mutations (22). In addition, the entropy of their vocalization temporal sequencing was reduced, consistent with increased stereotypy in their vocalizations.

To confirm and extend these results, we constructed mouse lines carrying other mutations found in human stuttering, including the Ser321Gly and Ala455Ser mutations in *Gnptab* (constructions detailed in *SI Appendix*, *SI Materials and Methods* and Fig. S1). With these mice, we first focused on analyses of pause durations in their USVs at P8. We calculated the mean pause lengths in each individual animal and compared the average of the individual mean pause lengths in each genotype group.

Pause lengths were classified into 2 types, interbout and intrabout pauses (*SI Appendix*, Fig. S2*A*). Interbout pauses are long pauses between groups of consecutive syllables (bouts), while intrabout pauses are short pauses between vocalization syllables within bouts (22). Interbout and intrabout pauses were determined by cutoffs calculated according to histograms of pause distributions (*SI Appendix*, Fig. S2*B*) (11, 22, 25). Previous studies showed that a key factor contributing to the increased pause durations in the vocalizations of *Gnptab* mut/mut animals is an increase in the interbout pause durations (22). In Ser321Gly mut/mut animals, the interbout pause durations were significantly longer than those of wild-type littermates ($P = 0.00056$, n of syllables > 15) (Fig. 1*A*). Animals with very low levels of vocalization overall produced data with very large apparent interbout pause values. To address potential bias from the inclusion of such animals, we also analyzed the USV recording data using a higher syllables cutoff value. A significant increase in pause durations was detected in mut/mut animals compared to wild-type littermates using this higher syllable cutoff as well ($P = 0.040$, n of syllables > 50) (Fig. 1*B*). As expected from the increase in the duration of long pauses, the number of bouts per recording was significantly decreased in the mut/mut animals compared to their wild-type littermates (*SI Appendix*, Fig. S3 *A* and *D*). However, in contrast to previous studies, we also found that the Ser321Gly mut/mut mice showed a small but significant increase in the duration of short pauses within vocalization bouts, known as intrabout pauses [mean of $^{+/+} = 0.149$, mut/mut = 0.156, $P = 0.010$ for n of syllables > 15 (Fig. 1*E*); mean of $^{+/+} = 0.149$, mut/mut = 0.154, $P = 0.040$ for n of syllables > 50 (Fig. 1*F*)]. The total number of syllables produced by Ser321Gly mut/mut animals was significantly less than that of their wild-type littermates (*SI Appendix*, Fig. S3 *B* and *E*). This was due to longer pause lengths between vocalizations, because vocalization durations (syllable lengths) did not differ between mutant and wild-type groups (*SI Appendix*, Fig. S3 *C* and *F*). Increased pause durations were observed in the mut/mut animals in 4 replicate trials. Measures of increased duration displayed a trend toward significance in trials 2 and 4, and reached significance in trials 1 and 3 (*SI Appendix*, Fig. S4), supporting the conclusion that *Gnptab* Ser321Gly mut/mut mice produce vocalizations with longer pauses.

The vocalizations of the *Gnptab* Ala455Ser mice displayed a slightly different phenotype. They did not show a significant difference when we used 15 as the minimal syllable cutoff value (Fig. 1*C*), although this value did become significantly different when we used 50 as syllables as our cutoff ($P = 0.0027$) (Fig. 1*D*). Intrabout pause duration analysis did not reach statistical significance (Fig. 1 *G* and *H*).

In addition to differences in vocalization timing, our previous study showed that *Gnptab* mut/mut mice exhibit higher stereotypy in the temporal sequencing of their vocalizations, as revealed by reduced temporal entropy in their vocalizations (22). To test whether Ser321Gly mut/mut mice also have such vocalization abnormalities, we analyzed both the usage and temporal sequencing of syllable types as categorized by an established classification scheme based on presence and size of abrupt pitch jumps (Fig. 2*A*) (11). As in the previous study, we found no statistically significant differences in the syllable types and their rates of usage between Ser321Gly mut/mut and their wild-type littermates (Fig. 2*B*). We tested the temporal diversity of the sequence of vocalizations using a first-order Markov process model, which compares the entropy present in the temporal structure of these vocalizations. We found significantly decreased entropy in the temporal structure in Ser321Gly mut/mut compared to wild-type ($P = 0.0064$) (Fig. 2*C*), which indicates that the Ser321Gly mut/mut mice exhibit greater stereotypy in temporal sequence, consistent with findings in previous studies. A higher degree of stereotypy in vocalizations can result from an increased repetition of syllables. We found no significant increase in the presence of doublet repetitions in the vocalizations of Ser321Gly mut/mut. However, there may be a trend toward an increased percentage of such doublets in the Ser321Gly mutant animals ($P = 0.13$, mean of $^{+/+} = 0.591$, mut/mut = 0.638) (Fig. 2*D*). A similar analysis was performed on the vocalizations of the Ala455Ser mice. These analyses showed that the mut/mut animals also displayed slightly reduced temporal entropy, although this difference did not reach statistical significance (*SI Appendix*, Fig. S5).

Taken together, the above findings indicate that mice carrying human stuttering-associated mutations produce vocalizations with longer pauses between syllables or bouts of syllables, and exhibited higher stereotypy in the temporal sequence of their vocalizations compared to wild-type littermates. These findings are consistent with the abnormal vocalization phenotype previously found in mutant mice carrying a different human stuttering-associated mutation (22). Because the vocalization phenotype in the Ser321Gly is more pronounced than that in Ala455Ser mouse, we focused on Ser321Gly mice for subsequent studies on the neuropathology of stuttering caused by this mutation.

Plasma Levels of Several Acid Hydrolases Are Elevated in *Gnptab* Ser321Gly Mice. In humans, homozygous loss-of-function mutations in *GNPTAB* cause mucolipidosis types II and III, in which the lack of the mannose 6-phosphate targeting signal results in abnormal accumulation of lysosomal enzymes in the plasma (26, 27). Mice totally deficient in GlcNAc-1-phosphotransferase activity display several symptoms similar to those seen in humans with mucolipidosis types II and III. For example, Gnptab knockout mice exhibit a 7- to 14-fold increase in plasma levels of lysosomal acid hydrolases when the ability to synthesize the Man-6-P recognition marker is missing (27). To assess whether missense mutations found in human stuttering give rise to a similar phenotype in mice, the activity of 5 acid hydrolases was measured in the plasma of the Ser321Gly mice and compared with wild-type

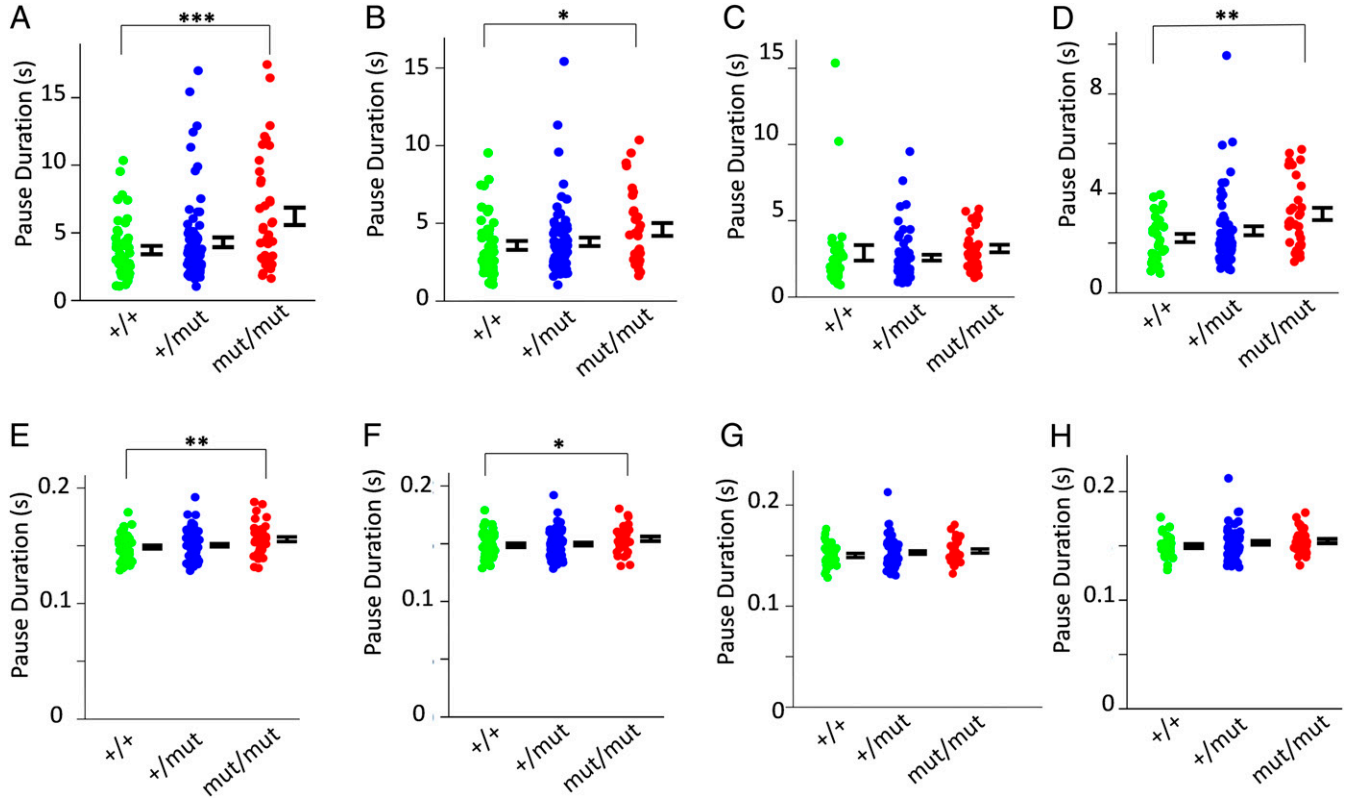

Fig. 1. Increased pause durations in the vocalizations of *Gnptab* Ser321Gly (S321G) and Ala455Ser (A455S) compared to wild-type littermates. All graphs indicate pause lengths in vocalizations of individual animals (1 point = 1 animal). The average of individual mean pause lengths in each genotype group was compared by *t* test calculating 2-tailed *P* value. Green represents wild-type ($^{+/+}$), blue represents heterozygous knockin (+/mut), red represents homozygous knockin (mut/mut). All *P* values depicted in the figures are comparison between $^{+/+}$ and mut/mut. $*P \leq 0.05$; $**P \leq 0.01$; $***P \leq 0.001$. Error bars indicate the SEM. (*A*) Interbout pause duration analysis in S321G animals displaying $n > 15$ syllables. Sample sizes (*n*) of $^{+/+}$ = 46, *n* of +/mut = 75, *n* of mut/mut = 40. (*B*) Interbout pause duration analysis with animals displaying total $n > 50$ syllables. The *n* of $^{+/+}$ = 45, *n* of +/mut = 71, *n* of mut/mut = 32. (*C*) Interbout pause duration analysis in A455S animals displaying $n > 15$ syllables. The *n* of $^{+/+}$ = 31, *n* of +/mut = 63, *n* of mut/mut = 30. (*D*) Interbout pause duration analysis in A455S animals displaying $n > 50$ syllables. The *n* of $^{+/+}$ = 29, *n* of +/mut = 62, *n* of mut/mut = 30. (*E*) Intrabout pause duration analysis in S321G animals displaying total $n >$ 15 syllables. The number of animals of each genotype are the same as that in *A*. (*F*) Intrabout pause duration analysis in S321G animals displaying total $n > 50$ syllables. The number of animals of each genotype are the same as that in *B*. (*G*) Intrabout pause duration analysis in A455S animals displaying total $n > 15$ syllables. The number of animals of each genotype are the same as that in *C*. (*H*) Intrabout pause duration analysis in A455S animals displaying total $n > 15$ syllables. The number of animals of each genotype are the same as that in *D*. Degrees of freedom (DF) in *A* and *E* is 84, in *B* and *F* is 75, in *C* and *G* is 59, in *D* and *H* is 57.

(Table 1). Although not as high as that in knockout mice, *Gnptab* Ser321Gly animals displayed a significant 1.26- to 3.3-fold increase in the plasma activity level of over that in wild-type mice for β-hexosaminidase, α-mannosidase, and β-mannosidase in both male and female groups (Table 1). There was no significant difference in the plasma activity levels of β-galactosidase and β-glucuronidase between Ser321Gly and wild-type mice. These data indicate that these missense mutations have functional effects on the biological activity of the lysosomal targeting function in these mice.

Nonvocal Behaviors in *Gnptab* Ser321Gly Mice. To examine whether Ser321Gly mut/mut mice exhibit any phenotypic anomalies beyond impaired vocalizations, we performed a battery of nonvocalization behavioral tests on adult animals. First, we measured spontaneous locomotion and exploratory behaviors in a 1-h open-field test. In previous studies, it was shown that *Gnptab* Glu1179-Lys homozygous mutant mice exhibited changes on 2 nonvocal behavioral measures, spontaneous locomotion and olfactory exploration (22), although these were not significantly different from controls when a Bonferonni correction was applied for the multiple behavioral tests performed. Here, we first measured spontaneous locomotion and exploratory behaviors in a 1-h open-field test. We found no significant genotypic differences in locomotor activity in Ser321Gly and wild-type animals (Fig. 3*A*). Measures of grip strength and prepulse inhibition of acoustic startle response also failed to show any significant differences between genotypes (Fig. 3 *B* and *E*). To measure balance and motor function, accelerating rotarod tests were performed over 3 successive days. Two-way ANOVA revealed no significant genotype effect ($P = 0.28$) (Fig. 3*C*), and the Kolmogorov–Smirnorv test also showed no significant difference between the 2 genotype groups ($P = 0.16$).

We then measured nose poking and olfactory exploration of Ser321Gly mice for both empty and odorant-containing holes compared to wild-type littermates (22), using chambers having both novel and familiar odorants. The duration of time spent with home-cage materials (familiar odor) or coconut (novel odor) was calculated and compared between wild-type and mutant mice. Two-way ANOVA revealed that both wild-type and Ser321Gly mice spent more time exploring the familiar odor than the novel odor ($P < 0.0001$), but this preference did not differ by genotype (Fig. 3*D*). These data suggest that this stuttering-causal mutation does not have any effect on exploratory activity guided by olfactory function.

We next examined social preference in our mice by measuring their preference for social compared to nonsocial stimuli in a 3-chamber experiment. We found that Ser321Gly and wild-type mice both robustly preferred interacting with a novel mouse placed in a containment cup compared to an identical cup that

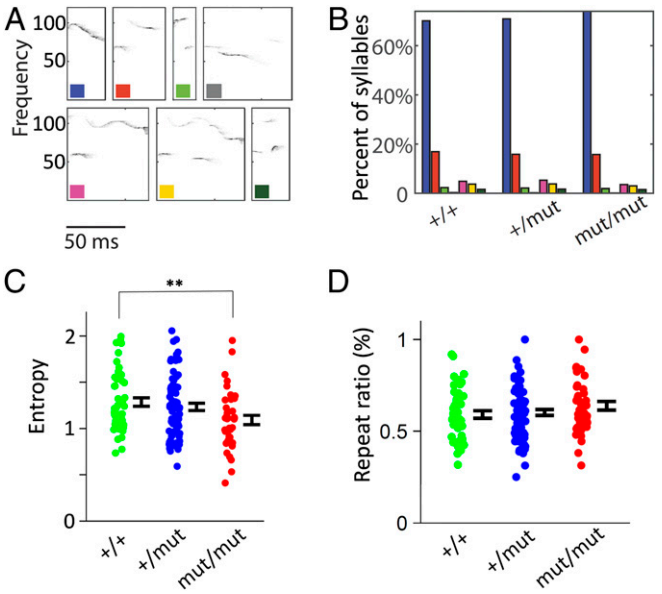

Fig. 2. Reduced entropy in the sequence of vocalizations of *Gnptab* Ser321Gly mice compared to wild-type littermates. (*A*) Sonograms of different syllable types. Syllable types were defined as previously described (20). (*B*) Percentage of times that 1 syllable type was followed by the same syllable type. Each color represents 1 syllable type as defined in *A*. (*C*) Diversity of vocalization sequences as quantified by the entropy of the corresponding first-order Markov process as previously described (20). (*D*) Proportion of repeated syllables (%). (*B–D*) Analyses of animals with syllable $n > 15$. The $^{+/+}$ and mut/mut were compared by *t* test calculating 2-tailed *P* value in *C* and *D*. Error bars indicate the SEM. $^{**}P \leq 0.01$. Samples sizes of each genotype are the same as that in Fig. 1 *A* and *C*. DF in *C* and *D* is 84. Mean entropy of $^{+/+}$ in *C* is 1.29 and that of mut/mut in *C* is 1.09.

did not contain a mouse, but there was no significant difference of interacting period between wild-type and mut/mut mice (Fig. 3*F*). Together, these results suggest that Ser321Gly does not cause global motor or cognitive deficits that could contribute to the impaired vocalizations that we observed.

Neuropathology Studies and Reduced Astrocyte Staining Density in *Gnptab* Ser321Gly Mice. Given the reproducible vocalization phenotype present in mice carrying different *Gnptab* mutations initially identified in humans who stutter, we sought to identify a specific neuropathology in these mice. Because the vocalization phenotype in the Ser321Gly is more pronounced than that in the Ala455Ser mice, we focused on Ser321Gly mice for subsequent studies of neuropathology associated with the vocalization deficit caused by this mutation. Because a histopathologic survey of brain and other tissue sections stained with H&E revealed no striking differences between homozygous mutant animals and wild-type, we investigated the brains of Ser321Gly mut/mut mice using immunohistochemistry with cell type-specific antibodies. These were chosen to interrogate major brain cell types and brain areas previously suggested to be sites of the primary neurological deficit in stuttering. Our first hypothesis was chosen based on imaging studies of the brains of humans who stutter, which have detected associations between stuttering and white matter deficits, including altered connectivity (10, 28, 29). White matter contains no neuronal cell bodies or synapses but does contain tightly packed glial cells, including oligodendrocytes (which produce myelin), astrocytes, and microglia. Astrocytes have been associated with developmental white matter disorders (30, 31), and pathological studies of *Gnptab* knockout mice showed demyelination (32) and microgliosis (32, 33). Based on this, we investigated the 3 glial cell types—astrocytes, oligodendrocytes, and microglial cells—in our *Gnptab* Ser321Gly mut/mut mice. Another major hypothesis regarding the genesis of stuttering involves functions of the basal ganglia (34, 35). Dopaminergic neurons form a major component of this brain region, and dopaminergic agents, such as risperidone and olanzapine, have been reported to improve fluency in some subjects who stutter (36–38). To investigate this, we studied $DRD2^{+}$ dopaminergic neurons in our mice. Yet another area of interest is the cerebellum, which is involved in fine motor control, and there have been reports that the cerebellum is involved in the neural pathway for speech production (39–41). In addition, a mouse model of developmental verbal dyspraxia caused by a mutation of *Foxp2* has been shown to have deficits of cerebellar Purkinje cells (42). Based on these findings, we also investigated cerebellar Purkinje cells in our mice. Brain tissues were stained with antibodies that include anti-glial fibrillary acidic protein (Gfap) to visualize astrocytes, anti-myelin basic protein (MBP) to visualize oligodendrocytes, anti-ionized calcium binding adaptor 1 (Iba1) to identify microglial cells, anti-calbindin (Calb1) to identify Purkinje cells of the cerebellum, and anti-tyrosine hydroxylase (TH) to identify dopaminergic neurons in the basal ganglia.

Astrocytes visualized by immunostaining with an anti-Gfap antibody were studied in the corpus callosum (CC) and hippocampal areas, which are known to have abundant astrocyte populations. To provide an anatomical landmark that allowed us to match the sectional position across brains, we compared hippocampal pyramidal layer staining in each brain section, and chose sections with similar morphology between mutant and wild-type (*SI Appendix*, Fig. S6). Coronal sections of brains from 5 mutant and wild-type pairs of P8 mice were used for staining and quantitation. We found the anti-Gfap–stained area, which represents the amount of astrocytes, was significantly reduced in

Table 1. Lysosomal enzyme activity in the plasma of *Gnptab* Ser321Gly mice

Animal group	β-Galactosidase	β-Glucuronidase	β-Hexosaminidase	β-Mannosidase	α-Mannosidase
Male					
Wild-type ($n = 9$)	24.95 ± 5	9.20 ± 1.8	206.73 ± 20	52.26 ± 3.7	117.33 ± 20.9
Ser321Gly ($n = 8$)	23.00 ± 6	7.72 ± 1.4	260.88 ± 35	112.39 ± 22.9	279.34 ± 77.1
P value	0.46	0.09	0.001	<0.0001	<0.0001
Female					
Wild-type ($n = 7$)	24.49 ± 3.9	8.70 ± 1.1	237.32 ± 17.3	36.12 ± 1.7	83.51 ± 10.8
Ser321Gly ($n = 7$)	28.00 ± 5.5	10.20 ± 2.0	390.81 ± 105.8	90.78 ± 11.1	272.3 ± 22.7
P value	0.19	0.12	0.0025	<0.0001	<0.0001
Merged					
Wild-type	24.75 ± 4.5	8.98 ± 1.6	220.11 ± 24.2	45.20 ± 8.8	102.53 ± 24.1
Ser321Gly	25.34 ± 5.9	8.87 ± 2.1	321.51 ± 99.5	102.30 ± 21.0	276.05 ± 56.6
P value	0.38	0.44	<0.001	<0.0001	<0.0001

Activity is expressed as nanomole 4-methyumbelliferone cleaved per hour per milliliter of plasma.

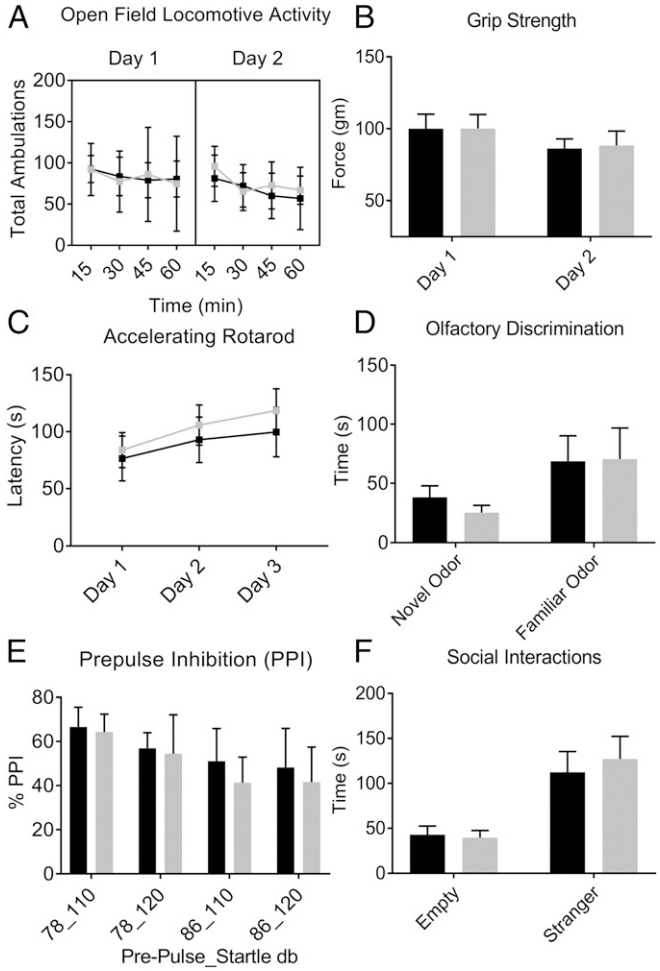

Fig. 3. Nonvocal behavioral tests of *Gnptab* Ser321Gly mice. Sixteen 7-mo-old Ser321Gly mut/mut mice and equal numbers of sex and age-matched $^{+/+}$ mice were used for 5 different nonvocal behavior tests, and 26 mut/mut and equal number of age-matched $^{+/+}$ mice were used for rotarod test. Black squares or bars indicate wild-type and gray squares or bars indicate *Gnptab* Ser321Gly mut/mut homozygotes. (*A*) One-hour open-field locomotive activity. (*B*) Grip strength. (*C*) Rotarod test with accelerating speed. (*D*) Olfactory discrimination. (*E*) Prepulse inhibition. (*F*) Social interaction. Error bars indicate the 95% confidence interval except for 1-h open-field locomotive activity test which has SD as error bars. DF is 50 for the rotarod test and 30 for all of the other tests.

the CC of the Ser321Gly mut/mut mice compared to that of wild-type littermates in all 5 pairs tested (*SI Appendix*, Fig. S7*A*; see also Fig. 5*A*). Quantification of the stained images shows that the difference in anti-Gfap–stained area between mutant and wild-type group is significant in both the left and right CC (fold-change in left: 26.3%; $P = 0.013$, fold-change in right: 19.5%, $P = 0.017$) (Fig. 4*A*). The anti-Gfap–stained area in the hippocampal subfield CA1 of Ser321Gly mut/mut was also lower than in wild-types, but this difference was smaller than that in the CC. (*SI Appendix*, Fig. S7*B*)

Because homozygous GNPTAB deficiency in humans and mice leads to progressive degenerative effects on the nervous system (32, 33), we performed the same anti-Gfap immunostaining in 3 pairs of older (16 mo of age) Ser321Gly mut/mut animals and their wild-type littermates, to see if there were any age-associated degenerative effects on the amount of astrocyte staining. Results from these 3 brain pairs showed a lower amount of astrocyte staining in CC of Ser321Gly mut/mut animals compared to wild-type, and this difference was highly significant (Fig. 4*B* and *SI Appendix*, Fig. S8). This difference was greater than that in P8 mice, suggestive of an astrocyte deficit that worsens with age in these mice.

No Differences in Staining of Other Brain Cells in *Gnptab* Ser321Gly Mice. Next, we measured the density of microglial cells in the CC and hippocampal areas of P8 mice using immunostaining with anti-Iba1 antibody. Anti-Iba1 staining area in the CC was similar to that in the hippocampus (*SI Appendix*, Fig. S9) and there was no difference in the cell area stained between Ser321Gly mut/mut and wild-type littermates (Fig. 5*A* and *SI Appendix*, Fig. S9). We also studied these tissues in adult animals (16 mo of age) and found no difference in the amount of anti-Iba1 staining area between the mutant and wild-type groups (*SI Appendix*, Fig. S10*A*).

Anti-MBP antibody was used to stain myelin-containing oligodendrocytes in the CC area. We found no significant difference in the area stained with anti-MBP between P8 homozygous mutant animals and their wild-type littermates (Fig. 5*B*). In adult mice, the anti-MBP staining was too saturated (*SI Appendix*, Fig. S10*B*) to quantify. To address this, we also used Luxol fast blue staining to visualize myelin in adult mouse brains and found no significant difference in these areas between mutant and wild-type mice (*SI Appendix*, Fig. S10*C*).

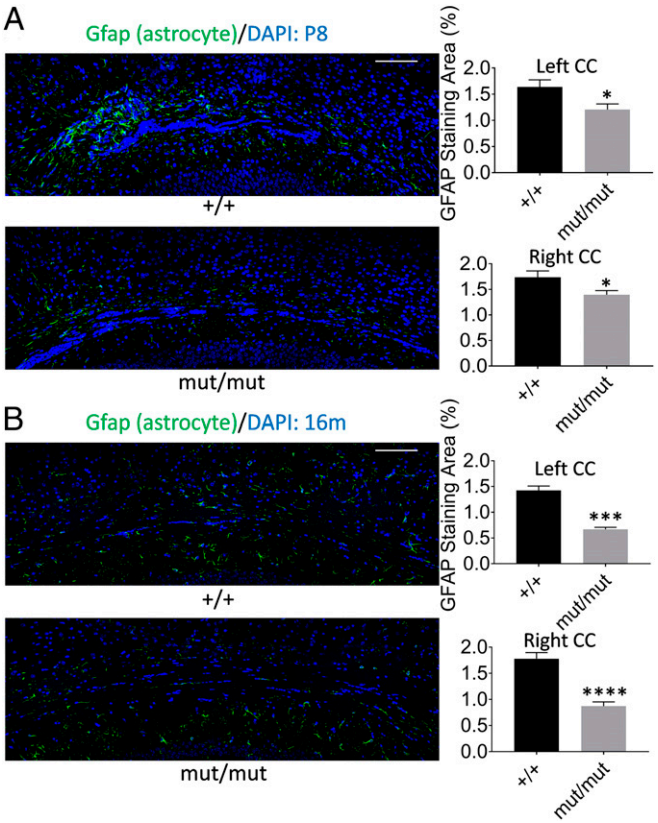

Fig. 4. Reduced astrocyte staining in the CC of *Gnptab* Ser321Gly mouse brains. Perfusion-fixed coronal cryosections (10-μm thickness) were used for immunostaining using anti-Gfap staining for astrocytes in the CC area. Quantification of the stained area was done using ImageJ software and paired *t* tests were used to test statistical significance of staining differences between genotype groups by calculating 2-tailed *P* values. (*A*) Immunostaining and quantitation of the stained area in P8 mice. Sample sizes (*n*) of $^{+/+}$ = 10, *n* of mut/mut = 10, DF is 9 for both hemispheres. (*B*) Immunostaining and quantitation of the stained area in 16-mo-old mice. The *n* of $^{+/+}$ = 8, *n* of mut/mut = 8, DF is 7 for left hemispheres. The *n* of $^{+/+}$ = 9, *n* of mut/mut = 8, DF is 8 for right hemispheres. (Scale bars, 100 μm.) Error bars indicate the SEM. $*P \leq 0.05$; $***P \leq 0.001$; $****P \leq 0.0001$.

Because stuttering represents a specialized motor control problem, we also examined cerebellar structures. We compared numbers of cerebellar Purkinje cell bodies in mutant and wild-type animals using immunostaining with anti-Calb1 antibody. A granular layer in the same lobule (the junction between lobule IV-V and the simple lobule, http://atlas.brain-map.org) of the cerebellum was chosen for comparison between mutant and wild-type. The number of anti-Calb1-stained cell bodies was counted and compared between mutant and wild-type pairs. The number of Purkinje cell bodies showed no difference between the 2 genotype groups in both P8 (Fig. 5*C*) and adult mice (*SI Appendix*, Fig. S10*D*).

Finally, dopaminergic neurons in striatum were stained with anti-TH antibody in P8 mice. Because the staining tended to be saturated across a network of nerve cells in this tissue, it was difficult to identify a difference at the level of light microscopy between the 2 genotype groups. However, quantification analysis showed no significant difference of staining area between the 2 genotypic groups in both P8 (Fig. 5*D*) and adult mice. (*SI Appendix*, Fig. S10*E*).

Detection of a White Matter Deficit in *Gnptab* Ser321Gly Mice. Because diffusion tensor imaging (DTI) has been shown to be sensitive to subtle differences in the white matter tissue environment, and because DTI scalars are known to change during postnatal white matter development and maturation in humans and rodents (43), we performed high-resolution, high-quality 14.1 Tesla DTI mapping in whole-brain fixed tissue specimens from P8 Ser321Gly mut/mut mice and their wild-type littermates. Details of DTI scanning and analysis procedures were described in *SI Appendix*, *SI Materials and Methods*. There were no gross morphologic differences between Ser21Gly mut/mut and wild-types by brain qualitative inspection (*SI Appendix*, Fig. S11), and most of DTI values—such as fractional anisotropy, trace, axial diffusivity, and radial diffusivity after registration were not significantly different between mut/mut and $^{+/+}$ littermates (Fig. 6). However, the template-based region-of-interest (ROI) analysis of LogJ showed significantly reduced local volume of the genu of the CC (mean ± SEM in $^{+/+}$ = −0.017 ± 0.011, mut/mut = −0.16 ± 0.012, $P = 0.025$) and no significant difference of the anterior commissure ($P = 0.26$), the splenium ($P = 0.67$), and the hippocampus ($P = 0.97$) of mut/mut brains compared to those of their $^{+/+}$ littermates (Fig. 6).

Abnormal Vocalization in Astrocyte-Specific *Gnptab* Knockout Mice. Our immunostaining data suggested that mice that carry human stuttering mutations and have abnormal vocalizations also have alterations specifically in their brain astrocytes. To independently test this hypothesis, we knocked out the *Gnptab* gene in specific brain cell types using mice that express Cre recombinase under the control of different brain cell type-specific promoters. We constructed an astrocyte-specific knockout of *Gnptab* as well as oligodendrocyte-specific, Purkinje cell-specific, and dopaminergic neuron-specific knockouts of *Gnptab*, and measured the vocalizations in P8 animals carrying these cell type-limited mutations.

We chose brain-specific Cre-driver mouse lines from the GENSAT Project at The Rockefeller University as follows: Gfap-Cre for astrocyte-specific expression of Cre, Adroa2a-Cre for dopaminergic Drd2 receptor-specific neurons in striatum, Pcp2-Cre for expression of Cre in cerebellar Purkinje cells, and Plp1-Cre for Cre expression in oligodendrocytes. Expression of the Cre recombinase in each mouse line was previously confirmed using an enhanced green fluorescent protein reporter in P7 mice and reported in the GENSAT database (http://www.gensat.org/cre.jsp) (*SI Appendix*, Fig. S12).

We constructed conditional knockout mice carrying the loxP sequence in the 5′ and 3′ flanking regions of exon 2 of *Gnptab*. The *Gnptab* with floxed exon 2 was designed to be located on

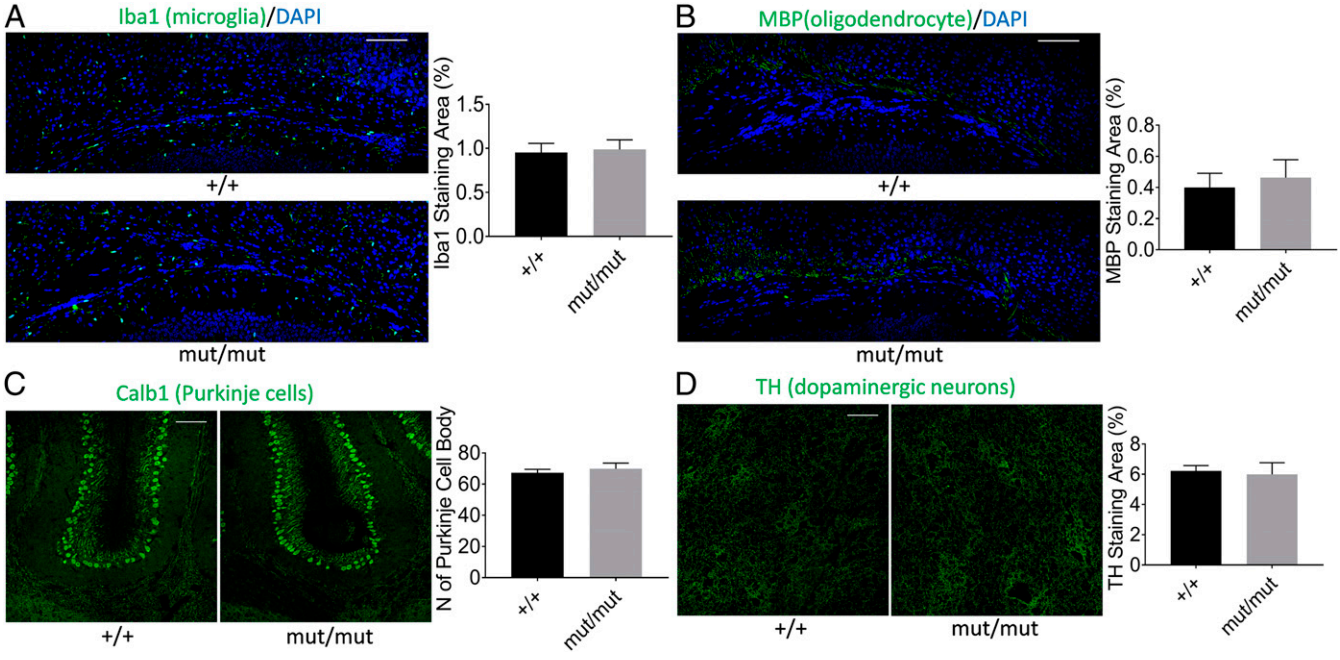

Fig. 5. No significant effect of the *Gnptab* Ser321Gly mutation on immunoreactivities in nonastrocyte cell types. (*A*) Immunostaining of microglial cells in the CC area with anti-Iba1 and quantitation of stained area. Sample sizes (*n*) of $^{+/+}$ = 5, *n* of mut/mut = 5, DF is 4. (*B*) Immunostaining of oligodendrocytes in CC area with anti-MBP and quantitation of stained area. The *n* of $^{+/+}$ = 6, *n* of mut/mut = 6, DF is 5. (*C*) Immunostaining of cerebellar Purkinje cells with anti-Calb1 and quantitation of stained area. The *n* of $^{+/+}$ = 6, *n* of mut/mut = 6, DF is 5. (*D*) Immunostaining of dopaminergic neurons with anti-TH and quantitation of stained area. The *n* of $^{+/+}$ = 8, *n* of mut/mut = 8, DF is 7. (Scale bars, 100 μm.) Age of all mice is P8. All data were obtained from left hemispheres of coronal sections. Error bars indicate the SEM.

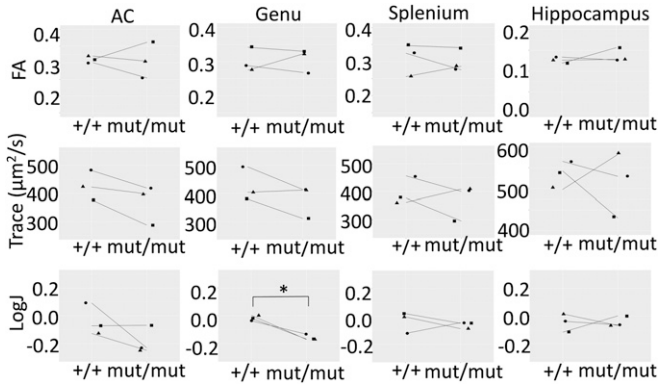

Fig. 6. Detection of a subtle white matter abnormality in *Gnptab* Ser321Gly mice by DTI. Quantitative analysis of template-based ROI values for fractional anisotropy (FA), Trace, and LogJ in the anterior commissure (AC), genu, splenium, and hippocampus are shown. Lines connect littermate pairs with the same sex and different genotype in the study. Three $^{+/+}$ and mut/mut pairs were marked as square, triangle, and circle. Paired *t*-tests were used to test significance by calculating 2-tailed *P* values. LogJ at the genu was significantly different between $^{+/+}$ and mut/mut. $*P \leq 0.05$. DF of each analysis is 2.

one chromosome, while the other chromosome had either the wild-type or fully deleted exon 2 in order to maximize the recombinase efficiency for deletion of the exon in the specific cells (*SI Appendix*, Fig. S13). Pup isolation calls at day P8 were recorded and analyzed using the same methods used for those of Ser321Gly and Ala455Ser knockin mice.

Gfap-specific *Gnptab* knockout mice showed significantly increased interbout pause durations in the conditional heterozygote knockouts (cHET) ($P = 0.05$), and a trend toward increased interbout durations in conditional homozygote knockouts (cHOM), although this difference did not reach statistical significance ($P = 0.09$, mean of wild-type = 2.33, cHOM = 3.04) (Fig. 7*A*). To confirm the astrocyte-specific knockout of *Gnptab* in mutant mice, we examined the colocalization of anti-Gnptab staining and anti-Gfap staining in P8 mice of cHOM and wild-type. In wild-type mice, anti-Gnptab staining labeled 36.6 ± 3.1% of the Gfap-staining area, but the anti-Gnptab staining labeled 15.3 ± 2.4% of the Gfap-staining area in cHOM mice (Fig. 7*E*). This difference between wild-type and cHOM was highly significant ($P = 0.0001$) (Fig. 7*E*), and supports the conclusion that Gnptab was selectively knocked out in the astrocytes of these mice.

We found no significant differences in interbout pause durations between oligodendrocyte, Drd2 neuron, and Purkinje cell-specific *Gnptab* knockout mice and their wild-type littermates (Fig. 7 *B–D*). Thus, 2 different experimental approaches, immunohistochemistry and brain cell type-specific expression of *Gnptab* mutations, indicate that a deficit in astrocytes, and not in other brain cell types previously proposed to be involved in the etiology of stuttering, underlies the altered vocalizations in mice carrying human stuttering mutations.

Discussion

Stuttering is characterized by interruptions in the flow of speech. The temporal characteristics of pauses in USVs of mutant mice are similar to those identified in the speech of humans who stutter and carry mutations in the *GNPTAB* gene (22). We show here that, in addition to the single mutation studied previously, 2 other *Gnptab* mutations initially identified in humans who stutter (Ser321Gly and Ala455Ser) also result in abnormal pauses in the USV of mice who carry them. These mice also display reduced temporal entropy in their vocalizations, consistent with increased stereotypy in these vocalizations. Thus, mice carrying human stuttering mutations in *Gnptab* present an animal model that recreates 2 core phenotypic features of human stuttering. Mouse models of other inherited speech disorders have been created, for example using mutations in *FOXP2*, and these mutations cause an absence of vocalizations in pups (42, 44). More recent work has shown that a *Foxp2* mutation can produce a vocalization syntax deficit in adult male mice, with deficits in the production of more complex USV sequences in social contexts, and that this is accompanied by a shift in the position of the laryngeal motor cortex layer-5 neurons in these animals (19). Humans and song-learning birds share characteristic features that include a forebrain system for vocal modification and auditory feedback (45). Because mice have been shown to possess limited vocal modification ability and some neuroanatomical features found in humans and song-learning birds (18), these findings and the present study show that mice can be used as model animals to investigate human speech disorders and also suggest a deep evolutionary conservation of some of the neural mechanisms involved in vocalization.

In humans, homozygous loss-of-function mutations in *GNPTAB* cause mucolipidosis types II and III, which are lysosomal storage disorders characterized by an abnormal presence of lysosomal hydrolases in the circulating plasma (46–48). In our *Gnptab* Ser321Gly mice, we found abnormal plasma levels in 3 of the lysosomal hydrolases tested. In contrast to mucolipidosis patients, humans who stutter and carry mutations in this gene typically have missense mutations and do not display any symptoms of mucolipidosis (3, 4). Although the mice carrying the missense mutation displayed moderate elevations of these lysosomal hydrolases, there were no signs of mucolipidosis in a wide range of tissues, and other than their USVs, their behavior was normal in a wide range of behavioral assays.

We have investigated the pathology that underlies the vocalization deficit in these mice at molecular, cellular, and anatomic scale. While an animal-wide pathology evaluation failed to show a difference in the *Gnptab* knockin animals by traditional H&E staining, a more detailed immunohistochemical study of the brains of these animals revealed one significant difference between them and their wild-type littermates, which was a deficit in staining with an anti-Gfap antibody, a classic marker of astrocytes. This deficit was especially prominent in the CC. Notably, we found no difference in staining with anti-Calb1, which is specific for Purkinje cells that are a major component the cerebellum. Deficits in this brain region, which plays a major role in the control of motor function, are prominent in mice carrying *FOXP2* mutations (42). The normal staining of Purkinje cells in our mice further reinforces the view that stuttering is both genetically (49) and pathologically distinct from developmental verbal dyspraxia, such as that associated with *FOXP2* mutations.

The involvement of an abnormality in astrocytes in the mouse vocalization deficit was supported by our studies of neural Cre-driver lines. We generated 4 such conditional knockout lines that expressed this *Gnptab* mutation solely in astrocytes, oligodendrocytes, Purkinje cells, or dopaminergic neurons, respectively. Of these, only the astrocyte-specific *Gnptab* knockout displayed a vocalization phenotype that was significantly different from their wild-type littermates. This phenotype consisted of more pauses and abnormally long pauses in their vocalizations, similar to the vocalization deficit in the whole-animal *Gnptab* knockin mutations.

Astrocytes have a wide range of critical roles in brain homeostasis (50), which include nutrient support for neurons (51), uptake and modulation of synaptic transmitter such as glutamate (52, 53), regulation of potassium concentration of extracellular space (54), and nervous system repair (55). While astrocyte deficits have not previously been suggested to be associated with stuttering, recent results have shown that these cells play an active role in the pathogenesis of neurological disorders (30, 31, 56). One of these studies reported that astrocytes are involved in pathological activation of lysosomal disorders by a noncell-autonomous functional pathway (30), which would be consistent with astrocytes

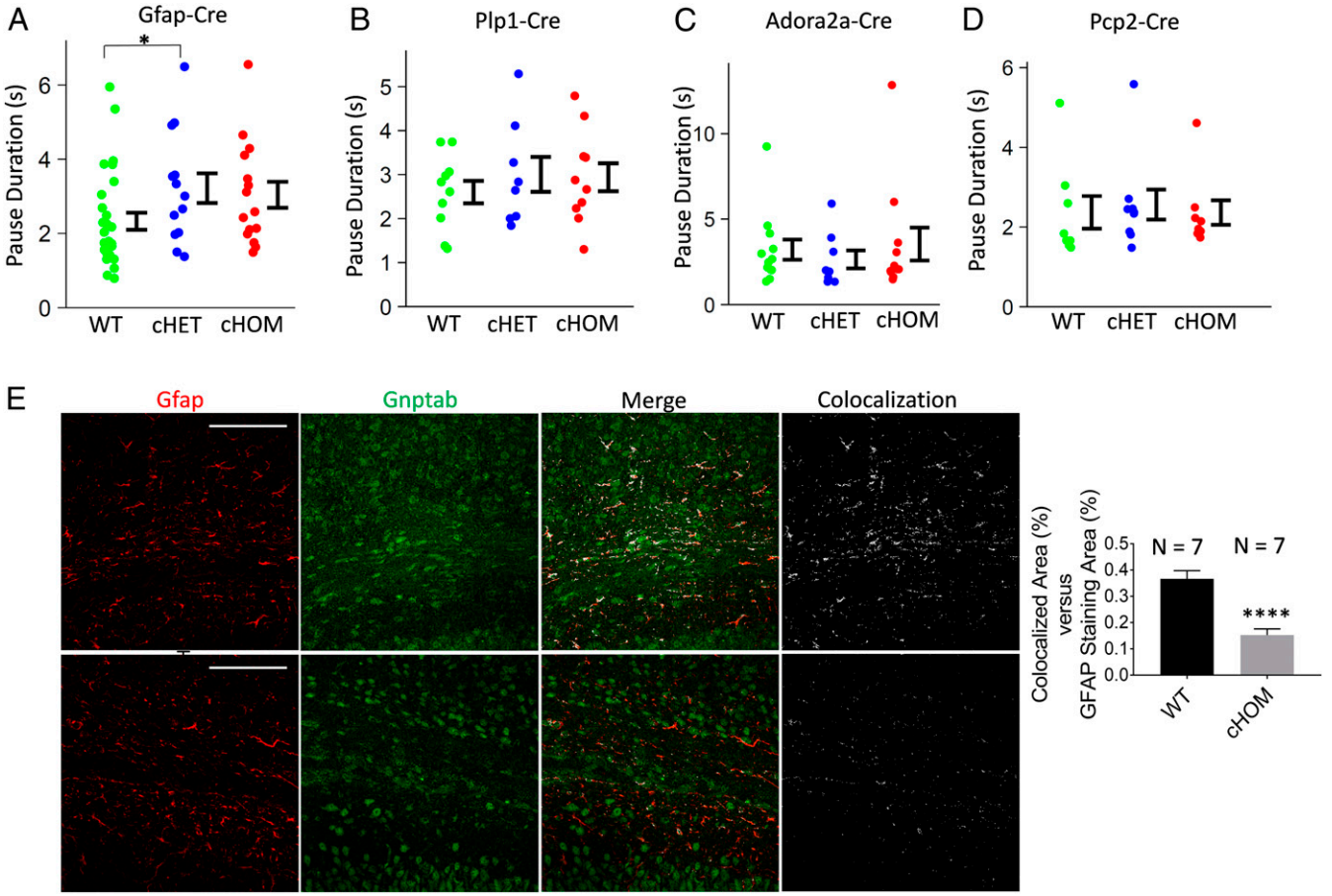

Fig. 7. Pause duration analysis in the vocalizations of brain cell type-specific *Gnptab* knockout mice compared to wild-type littermates. The average of individual mean pause lengths in each genotype group was compared by *t* test calculating 2-tailed *P* value. $*P \leq 0.05$; $****P \leq 0.0001$. Error bars indicate the SEM. (*A*) Interbout pause duration analysis In Gfap Cre-driver (astrocyte-specific) *Gnptab* knockout mice. Sample sizes (*n*) of wild-type animals = 29, *n* of cHET animals = 13, and *n* of cHOM animals = 15. (*B*) Interbout pause duration analysis in Plp1 Cre-driver (oligodendrocyte-specific) *Gnptab* knockout mice. The *n* of wild-type animals = 10, *n* of cHET animals = 8, *n* of cHOM animals = 10. (*C*) Interbout pause duration analysis in Adora2a Cre-driver (Drd2 neuron-specific) *Gnptab* knockout mice. The *n* of WT animals = 12, *n* of cHET animals = 8, *n* of cHOM animals = 11. (*D*) Interbout pause duration analysis in Pcp2 Cre-driver (Purkinje cell-specific) *Gnptab* knockout mice. The *n* of WT animals = 8, *n* of cHET animals = 9, *n* of cHOM animals = 8. Number of syllables cutoff for *A*–*D* is 15. (*E*) Immunostaining of CC area with anti-Gfap (red) and anti-Gnptab (green) in cHOM (*Bottom*) and wild-type littermates (*Top*) and quantification of stained area. White color indicates areas of colocalization, which was analyzed using the "Colocalization" plugin (https://imagej.nih.gov/ij/plugins/colocalization.html) in ImageJ software with default threshold. Quantification of immunostaining area in which ratio of colocalization area versus Gfap staining area was calculated. (Scale bars, 100 μm.) Sample size for quantification of immunostaining is depicted on top of each bar graph.

being involved in pathogenesis of human stuttering caused by a deficit in lysosomal targeting functions. Previous studies have shown that levels of astrocytes and microglial cells are increased in adult mice carrying a knockout mutation of *Gnptab*, which is model of mucolipidosis type II (32, 33). These studies demonstrated that astrogliosis and inflammation causing neurodegeration are activated by this complete knockout of Gnptab, which is associated with systemic pathologies. However, our data showed that astrocyte levels of 16-mo-old mutant mice carrying *Gnptab* Ser321Gly are still lower than those in wild-type littermates. This result suggests that partial deficit of lysosomal targeting function caused by a missense mutation in *Gnptab* is not associated with increased astrogliosis and inflammation, but rather is associated with a loss of other physiological functions of astrocytes.

The most prominent location of astrocyte pathology we observed by immunohistochemistry was in the CC. The CC connects the 2 hemispheres of the brain, and abnormalities in interhemispheric functions has been previously suggested to be associated with stuttering (57). DTI analysis also suggested a potential reduction in local volume of the CC in *Gnptab* Ser321Gly mice. A location for the site of the functional deficit in the CC in our mutant mice is consistent with recent results from brain structural imaging studies in children who stutter, a recent study of which showed abnormalities of connectivity in the CC. These were particularly notable in children with persistent rather than recovered stuttering (29). The human subjects with documented *GNPTAB* mutations to date all have persistent stuttering (3, 4). In addition, studies of our animal models show that astrocyte pathology persists into adulthood in these animals. Thus, human genetic findings (2), animal model studies, and independent human brain imaging studies (3, 4) now all support a role for a cellular deficit in the CC in the genesis of persistent developmental stuttering.

The present study suggests astrocytes as a previously unsuspected site of the pathophysiology underlying human stuttering. Because *Gnptab* is universally expressed in brain cells and tissues (49, 58, 59), a current question is why astrocytes present an increased susceptibility to pathology from partial loss of function mutations in *Gnptab* compared to other brain cell types. We note that our data do not completely rule out the possibility that other brain cells are involved in pathogenesis of stuttering associated with mutations in *Gnptab* (22). Also unknown are the precise mechanisms by which this Gnptab functional

deficit leads to our observed difference in astrocyte cellular density. However, our evidence for the involvement of this cell type and specific brain structure present new avenues for the understanding of cause of stuttering at anatomic, cellular, and molecular scales within the brain.

Materials and Methods

Animal Subjects. Mice were housed with 1 to 5 animals per cage in standard plastic home cages on a 12-h light/dark cycle, and all vocal or nonvocal behavioral experiments were performed during the light phase. All mice used in this study have C57BL/6J strain background. All experiments and maintenance of mice were conducted in accordance with the National Institutes of Health Guidelines for the Care and Use of Laboratory Animals, and were carried out under the National Institute on Deafness and other Communication Disorders Animal Care and Use Committee protocol #1318-16. One to 5 mice were housed per cage. In case of 5 males in a cage, they were separated into multiple cages at sexual maturity (6 to 8 wk) to prevent fighting.

Mouse Vocalization Recording and USV Analysis. USVs of mice were recorded on P8 using a recording system from Avisoft Bioacoustics (https://www.avisoft.com). A heterozygote × heterozygote breeding strategy was used to ensure the availability of wild-type littermate controls with matched pre- and postnatal environment. Foot tattoos were applied for temporary identification of pups 1 to 3 d before recording, prior to genotyping the animals. Animal vocalizations were recorded and vocalization data were analyzed blind to genotype. Before recording of pups, the dam mice were removed from their pups and the cage was kept on a warm heating pad during experiments. After an initial 10-min equilibrium period on the heating pad, the pup was transferred to the recording chamber and the body temperature of each pup was measured using an infrared thermometer. Vocalization recordings of each pup were done in a plastic 12.4-cm × 12.4-cm × 13.8-cm chamber for 5 min. After identification using the foot tattoo and measuring body weight, pups were returned to the dam. The pups were genotyped after weaning on P21. The USV data were analyzed using Matlab (Mathworks, https://www.mathworks.com/) including the signal-processing toolbox, image-processing toolbox, statistics and machine learning toolbox. For quantitative analysis, Matlab codes originally developed by T. Holy (11) and subsequently modified by T. Barnes (22) were used. Mean pause lengths between syllables (intrabout) or groups of syllables (interbout) in vocalizations of each genotype group were compared by *t* test and 2-tailed *P* value was used in each analysis. All experiments were done in 4 different stages, and both data of each stage and combined analysis data are shown.

Nonvocalization Related Behavior. Thirty-two mice, 16 *Gnptab* Ser321Gly mut/mut and 16 wild-type littermates, were tested at 7 mo of age on a battery of nonvocalization-related behaviors to assess spontaneous locomotion, forelimb strength, motor coordination, novelty seeking and aversion, social recognition memory, and paired-pulse inhibition. For the rotarod test, 10 *Gnptab* Ser321Gly mut/mut and 10 wild-type littermates were additionally tested. Experimental procedures for behavior tests are similar to previously described methods (22). Because mouse behaviors have been shown to be comparable in both light and dark phase (60), vocalization and behavioral tests were carried out exclusively in light phase to reliably standardize light exposure across all tests. The results are shown in Fig. 4 in the order that the tests were performed. Details of test procedures are described in *SI Appendix, SI Materials and Methods*.

Assay of Plasma Lysosomal Hydrolase Levels. Lysosomal hydrolase activities in plasma samples were determined by fluorometric enzyme assays as described previously (27). In brief, plasma samples were incubated with 5 mM 4-methylumbelliferyl-coupled specific substrates in a 50 mM citrate buffer containing 0.5% Triton X-100, pH 4.5, at 37 °C. Reactions were stopped by addition of 0.1 M glycine-NaOH solution, pH 10.3, and the fluorescence read at 495 nm. The plasma activities are expressed as nanomoles of hydrolyzed methylumbelliferone per hour per milliliter of plasma.

Antibodies and Immunostaining. Mice of the indicated ages were anesthetized and perfused through the heart with PBS and 4% paraformaldehyde (Electron Microscopy Sciences) and postfixed by immersion in 4% paraformaldehyde overnight at 4 °C. The brains were cryoprotected with PBS solution containing sucrose for 2 d (4 h in 10%, overnight in 20%, 24 h in 30% sucrose). Brain tissue mounts were prepared for cryosectioning using OCT media with isopentane solution chilled on dry ice. Ten-millimeter tissue sections were obtained using Cryostat (Leica CM3050S), mounted on positively charged glass slides (Superfrost Plus Gold; Thermo Fisher Scientific), then dried at room temperature for 20 min.

The tissue sections were stored at −80 °C until usage. Reagents for immunostaining were prepared according to methods described in IHC-World (http://www.ihcworld.com/protocol_database.htm). The following antibodies and dilutions were used for the immunostaining: rabbit anti-Gfap antibody (ab7260, 1:5,000; Abcam), rabbit anti-MBP antibody (ab40390, 1:1,000; Abcam), rabbit anti-Iba1 antibody (NBP2-19019, 1:100; Novus Biologicals), rabbit anti-TH antibody (ab112, 1:500; Abcam), rabbit anti-Calb1 antibody (ab49899, 1:100; Abcam), rabbit anti-Gfap antibody (BS-13476R, 1:200; Bioss Antibodies), chicken anti-Gfap antibody (ab4674, 1:4,000; Abcam), goat anti-Rabbit IgG H&L (Alexa Fluor 488) preadsorbed (ab150081,1:200; Abcam), and goat anti-chicken IgY H&L (Alexa Fluor 647) preadsorbed (ab150175,1:200; Abcam). Blocking agent treatment was performed for 30 min, followed by 16-h incubation with the primary antibodies. The antibodies were washed with PBS containing 0.05% Tween20 3 times in glass coplin jar (5 min, 15 min, 5 min). Slides were then incubated with the secondary antibody for 1 h and then washed with PBS 3 times (5 min, 15 min, 5 min). Vectashield HardSet Antifade mounting medium containing Dapi (H-1500, Vector Laboratory) was used for final mounting after staining. An LSM780 microscope (Zeiss) was used for the fluorescence microscopy. Quantification of images was done with ImageJ (https://imagej.nih.gov/ij). Because these samples represented both technical and biological replicates using a littermate of the same sex, a paired *t* test was used to test statistical significance in difference of quantified data between genotype groups by calculating 2-tailed *P* values.

Breeding Strategy for Brain-Cell Specific Gene Knockout Mice. To generate conditional knockout of *Gnptab* in specific brain cell types, embryonic stem cells carrying the loxP sequence fragment (ATAACTTCGTATAGCATACATTATACGAAGTTAT) in the flanking regions of exon 2 of *Gnptab* was purchased from EUCOMM [European Conditional Mouse Mutagenesis Program, https://www.mousephenotype.org, Allele name: Gnptab$^{tm1a(EUCOMM)Wtsi}$] (61) and germline transmission was achieved in collaboration with TAMC, as described above. B6.FVB background B6 (C3)-Tg(Pgk1-FLPo)10Sykr/J mice were mated with mice carrying the targeted gene cassette to remove the neomycin cassette. Transgenic mice expressing Cre recombinase under the control of different promoters (so called Cre-driver lines) were purchased from Jackson Laboratory [B6.Cg-Tg(Gfap-cre)77.6Mvs/2J, B6.129-Tg(Pcp2-Cre)2Mpin/J, B6.Cg-Tg(Plp1-cre/ERT)3Pop/J] or MMRRC [B6.FVB(Cg)-Tg(Adora2a-cre)KG139Gsat/Mmucd]. The GENESAT database (http://www.gensat.org/searchgenes.jsp) was used to check the targeted gene expression induced by each of the Cre-drivers (*SI Appendix*, Fig. S10). Heterozygote *Gnptab* whole knockout mice carrying *Cre* gene cassette were mated with homozygotes carrying a floxed exon 2 of *Gnptab* to get cell type-specific knockout on a single chromosome, which results in 4 different genotypes (*SI Appendix*, Fig. S13). USVs were tested with P8 pups using methods described above, and genotyping and USV analysis was done after weaning.

ACKNOWLEDGMENTS. We thank Dr. James McGehee and Patrick Diers for expert veterinary assistance; Dr. Matthew Starost for mouse pathology evaluations; Dr. Stuart Kornfeld for assistance with the plasma enzyme assays; Dr. Yogita Chudasama and Kevin David Cravedi for assistance with nonvocal animal behavior tests; the NIH mouse imaging facility, especially Dr. Jeeva P Munasinghe, for diffusion tensor imaging experiments; and Thomas Friedman and Doris Wu for valuable comments on the manuscript. This work was performed under National Institute on Deafness and other Communication DisordersAnimal Study Protocol 1318-16. This work was supported by the Intramural Research Program of the NIH, National Institute on Deafness and other Communication Disorders under intramural Grant Z1A-000046-18 (to D.D.), by the National Institute of Mental Health Rodent Behavioral Core and by the National Heart, Lung, and Blood Institute Animal MRI Core.

1. O. Bloodstein, N. B. Ratner, *A Handbook on Stuttering* (Thomson/Delmar Learning, Clifton Park, NY, ed. 6, 2008).
2. C. Frigerio-Domingues, D. Drayna, Genetic contributions to stuttering: The current evidence. *Mol. Genet. Genomic Med.* **5**, 95–102 (2017).
3. C. Kang *et al.*, Mutations in the lysosomal enzyme-targeting pathway and persistent stuttering. *N. Engl. J. Med.* **362**, 677–685 (2010).
4. M. H. Raza *et al.*, Association between rare variants in AP4E1, a component of intracellular trafficking, and persistent stuttering. *Am. J. Hum. Genet.* **97**, 715–725 (2015).
5. M. H. Raza *et al.*, Mucolipidosis types II and III and non-syndromic stuttering are associated with different variants in the same genes. *Eur. J. Hum. Genet.* **24**, 529–534 (2016).
6. J. Neefjes, R. van der Kant, Stuck in traffic: An emerging theme in diseases of the nervous system. *Trends Neurosci.* **37**, 66–76 (2014).

7. R. Salmelin *et al*., Functional organization of the auditory cortex is different in stutterers and fluent speakers. *Neuroreport* **9**, 2225–2229 (1998).
8. P. T. Fox *et al*., A PET study of the neural systems of stuttering. *Nature* **382**, 158–161 (1996).
9. A. L. Foundas, A. M. Bollich, D. M. Corey, M. Hurley, K. M. Heilman, Anomalous anatomy of speech-language areas in adults with persistent developmental stuttering. *Neurology* **57**, 207–215 (2001).
10. S. E. Chang *et al*., Anomalous network architecture of the resting brain in children who stutter. *J. Fluency Disord.* **55**, 46–67 (2018).
11. T. E. Holy, Z. Guo, Ultrasonic songs of male mice. *PLoS Biol.* **3**, e386 (2005).
12. J. M. Grimsley, J. J. Monaghan, J. J. Wenstrup, Development of social vocalizations in mice. *PLoS One* **6**, e17460 (2011).
13. M. L. Scattoni, J. Crawley, L. Ricceri, Ultrasonic vocalizations: A tool for behavioural phenotyping of mouse models of neurodevelopmental disorders. *Neurosci. Biobehav. Rev.* **33**, 508–515 (2009).
14. F. Hoffmann, K. Musolf, D. J. Penn, Spectrographic analyses reveal signals of individuality and kinship in the ultrasonic courtship vocalizations of wild house mice. *Physiol. Behav.* **105**, 766–771 (2012).
15. J. B. Panksepp *et al*., Affiliative behavior, ultrasonic communication and social reward are influenced by genetic variation in adolescent mice. *PLoS One* **2**, e351 (2007).
16. T. Kikusui *et al*., Cross fostering experiments suggest that mice songs are innate. *PLoS One* **6**, e17721 (2011).
17. H. Choi, S. Park, D. Kim, Two genetic loci control syllable sequences of ultrasonic courtship vocalizations in inbred mice. *BMC Neurosci.* **12**, 104 (2011).
18. G. Arriaga, E. P. Zhou, E. D. Jarvis, Of mice, birds, and men: The mouse ultrasonic song system has some features similar to humans and song-learning birds. *PLoS One* **7**, e46610 (2012).
19. J. Chabout *et al*., A Foxp2 mutation implicated in human speech deficits alters sequencing of ultrasonic vocalizations in adult male mice. *Front. Behav. Neurosci.* **10**, 197 (2016).
20. G. A. Castellucci, M. J. McGinley, D. A. McCormick, Knockout of Foxp2 disrupts vocal development in mice. *Sci. Rep.* **6**, 23305 (2016). Erratum in: *Sci. Rep.* **7**, 39722 (2017).
21. A. Fedyna, D. Drayna, C. Kang, Characterization of a mutation commonly associated with persistent stuttering: Evidence for a founder mutation. *J. Hum. Genet.* **56**, 80–82 (2011).
22. T. D. Barnes *et al*., A mutation associated with stuttering alters mouse pup ultrasonic vocalizations. *Curr. Biol.* **26**, 1–10 (2016).
23. J. A. Harris *et al*., Anatomical characterization of Cre driver mice for neural circuit mapping and manipulation. *Front. Neural Circuits* **8**, 76 (2014).
24. S. Gong *et al*., Targeting Cre recombinase to specific neuron populations with bacterial artificial chromosome constructs. *J. Neurosci.* **27**, 9817–9823 (2007).
25. J. Chabout, A. Sarkar, D. B. Dunson, E. D. Jarvis, Male mice song syntax depends on social contexts and influences female preferences. *Front. Behav. Neurosci.* **9**, 76 (2015).
26. M. Boonen, P. Vogel, K. A. Platt, N. Dahms, S. Kornfeld, Mice lacking mannose 6-phosphate uncovering enzyme activity have a milder phenotype than mice deficient for N-acetylglucosamine-1-phosphotransferase activity. *Mol. Biol. Cell* **20**, 4381–4389 (2009).
27. C. M. Gelfman *et al*., Mice lacking alpha/beta subunits of GlcNAc-1-phosphotransferase exhibit growth retardation, retinal degeneration, and secretory cell lesions. *Invest. Ophthalmol. Vis. Sci.* **48**, 5221–5228 (2007).
28. S. E. Chang, D. C. Zhu, A. L. Choo, M. Angstadt, White matter neuroanatomical differences in young children who stutter. *Brain* **138**, 694–711 (2015).
29. H. M. Chow, S. E. Chang, White matter developmental trajectories associated with persistence and recovery of childhood stuttering. *Hum. Brain Mapp.* **38**, 3345–3359 (2017).
30. C. Di Malta, J. D. Fryer, C. Settembre, A. Ballabio, Astrocyte dysfunction triggers neurodegeneration in a lysosomal storage disorder. *Proc. Natl. Acad. Sci. U.S.A.* **109**, E2334–E2342 (2012).
31. E. Sen, S. W. Levison, Astrocytes and developmental white matter disorders. *Ment. Retard. Dev. Disabil. Res. Rev.* **12**, 97–104 (2006).
32. K. Kollmann *et al*., Lysosomal dysfunction causes neurodegeneration in mucolipidosis II 'knock-in' mice. *Brain* **135**, 2661–2675 (2012).
33. R. A. Idol *et al*., Neurologic abnormalities in mouse models of the lysosomal storage disorders mucolipidosis II and mucolipidosis III γ. *PLoS One* **9**, e109768 (2014).
34. P. A. Alm, Stuttering and the basal ganglia circuits: A critical review of possible relations. *J. Commun. Disord.* **37**, 325–369 (2004).
35. J. Lan *et al*., Association between dopaminergic genes (SLC6A3 and DRD2) and stuttering among Han Chinese. *J. Hum. Genet.* **54**, 457–460 (2009).
36. G. A. Maguire, G. D. Riley, D. L. Franklin, L. A. Gottschalk, Risperidone for the treatment of stuttering. *J. Clin. Psychopharmacol.* **20**, 479–482 (2000).
37. G. A. Maguire *et al*., Olanzapine in the treatment of developmental stuttering: A double-blind, placebo-controlled trial. *Ann. Clin. Psychiatry* **16**, 63–67 (2004).
38. A. Boyd, K. Dworzynski, P. Howell, Pharmacological agents for developmental stuttering in children and adolescents: A systematic review. *J. Clin. Psychopharmacol.* **31**, 740–744 (2011).
39. H. Ackermann, The contribution of the cerebellum to speech and language. *Brain Lang.* **127**, 315–316 (2013).
40. D. E. Callan, M. Kawato, L. Parsons, R. Turner, Speech and song: The role of the cerebellum. *Cerebellum* **6**, 321–327 (2007).
41. J. R. Booth, L. Wood, D. Lu, J. C. Houk, T. Bitan, The role of the basal ganglia and cerebellum in language processing. *Brain Res.* **1133**, 136–144 (2007).
42. E. Fujita *et al*., Ultrasonic vocalization impairment of Foxp2 (R552H) knockin mice related to speech-language disorder and abnormality of Purkinje cells. *Proc. Natl. Acad. Sci. U.S.A.* **105**, 3117–3122 (2008).
43. H. Huang, A. Yamamoto, M. A. Hossain, L. Younes, S. Mori, Quantitative cortical mapping of fractional anisotropy in developing rat brains. *J. Neurosci.* **28**, 1427–1433 (2008).
44. W. Shu *et al*., Altered ultrasonic vocalization in mice with a disruption in the Foxp2 gene. *Proc. Natl. Acad. Sci. U.S.A.* **102**, 9643–9648 (2005).
45. E. D. Jarvis, Learned birdsong and the neurobiology of human language. *Ann. N. Y. Acad. Sci.* **1016**, 749–777 (2004).
46. M. Kudo, M. S. Brem, W. M. Canfield, Mucolipidosis II (I-cell disease) and mucolipidosis IIIA (classical pseudo-hurler polydystrophy) are caused by mutations in the GlcNAc-phosphotransferase alpha / beta -subunits precursor gene. *Am. J. Hum. Genet.* **78**, 451–463 (2006).
47. R. A. Steet *et al*., A splicing mutation in the alpha/beta GlcNAc-1-phosphotransferase gene results in an adult onset form of mucolipidosis III associated with sensory neuropathy and cardiomyopathy. *Am. J. Med. Genet. A.* **132A**, 369–375 (2005).
48. M. Encarnação *et al*., Molecular analysis of the GNPTAB and GNPTG genes in 13 patients with mucolipidosis type II or type III—Identification of eight novel mutations. *Clin. Genet.* **76**, 76–84 (2009).
49. T. U. Han *et al*., A study of the role of the FOXP2 and CNTNAP2 genes in persistent developmental stuttering. *Neurobiol. Dis.* **69**, 23–31 (2014).
50. M. Pekny, M. Nilsson, Astrocyte activation and reactive gliosis. *Glia* **50**, 427–434 (2005).
51. M. Bélanger, I. Allaman, P. J. Magistretti, Brain energy metabolism: Focus on astrocyte-neuron metabolic cooperation. *Cell Metab.* **14**, 724–738 (2011).
52. M. Santello, A. Volterra, Synaptic modulation by astrocytes via Ca2+-dependent glutamate release. *Neuroscience* **158**, 253–259 (2009).
53. R. Piet, L. Vargová, E. Syková, D. A. Poulain, S. H. Oliet, Physiological contribution of the astrocytic environment of neurons to intersynaptic crosstalk. *Proc. Natl. Acad. Sci. U.S.A.* **101**, 2151–2155 (2004).
54. W. Walz, Role of astrocytes in the clearance of excess extracellular potassium. *Neurochem. Int.* **36**, 291–300 (2000).
55. M. A. Anderson *et al*., Astrocyte scar formation aids central nervous system axon regeneration. *Nature* **532**, 195–200 (2016).
56. J. J. Rodríguez-Arellano, V. Parpura, R. Zorec, A. Verkhratsky, Astrocytes in physiological aging and Alzheimer's disease. *Neuroscience* **323**, 170–182 (2016).
57. Y. Kikuchi *et al*., Abnormal auditory synchronization in stuttering: A magnetoencephalographic study. *Hear. Res.* **344**, 82–89 (2017).
58. Y. Zhang *et al*., An RNA-sequencing transcriptome and splicing database of glia, neurons, and vascular cells of the cerebral cortex. *J. Neurosci.* **34**, 11929–11947 (2014).
59. Y. Zhang *et al*., Purification and characterization of progenitor and mature human astrocytes reveals transcriptional and functional differences with mouse. *Neuron* **89**, 37–53 (2016).
60. M. Yang, M. D. Weber, J. N. Crawley, Light phase testing of social behaviors: Not a problem. *Front. Neurosci.* **2**, 186–191 (2008).
61. W. C. Skarnes *et al*., A conditional knockout resource for the genome-wide study of mouse gene function. *Nature* **474**, 337–342 (2011).